

Original Research

Visualization of Aortic Valve Leaflets Using Black Blood MRI

Andrew E. Arai, MD,^{1*} Frederick H. Epstein, PhD,² Karen E. Bove, RT,¹
and Steven D. Wolff, MD, PhD,^{1,3}

Although magnetic resonance imaging (MRI) is capable of imaging various physiological parameters associated with the heart valves, it has generally been difficult to visualize the valve leaflets directly. The aortic valve was imaged in 120 patients referred for cardiac MRI to assess myocardial volumes or mass. The average patient age was 37 and ranged from 9 to 75 years. Heart rate ranged from 43 to 100 bpm. Imaging was performed on a 1.5 T scanner equipped with enhanced gradients and a cardiac phased-array coil. A double inversion recovery fast spin-echo sequence was used to acquire short-axis images of the aortic valve in a breathhold (15 ± 3 seconds). All three leaflets of the aortic valve were seen in 102 of 120 studies (85%). Two leaflets were detected in another 15 subjects. No leaflets were seen in three individuals. Seven cases of a bicuspid or thickened aortic valves were clearly distinguished from normal valves. The signal-to-noise ratio of aortic leaflets (14 ± 5) was significantly higher than that of the residual blood signal in the aortic root (7 ± 4 , $P < 0.001$). MR images showed the aortic valve leaflets in a high fraction of people with suspected normal aortic valves and detected seven cases of abnormal aortic valves. The potential of MRI to study both the anatomic and functional consequences of valvular heart disease warrants further study. *J. Magn. Reson. Imaging* 1999;10:771-777. © 1999 Wiley-Liss, Inc.

Index terms: magnetic resonance imaging; aortic valve; bicuspid aortic valve; pulmonic valve; mitral valve

ALTHOUGH echocardiography dominates the noninvasive evaluation of valvular heart disease clinically, MRI has many characteristics that make it particularly well suited to this patient population (1,2). For example, multiphase cine gradient recalled echo (GRE) imaging demonstrates flow-related signal voids near valves that

correlate well with the magnitude of regurgitation or stenosis as measured by color Doppler echocardiography (3-5) or cardiac catheterization (4,6,7). Velocity-encoded phase contrast MRI can delineate the regurgitant jet, quantify the velocity across a stenotic valve (8) or assess the regurgitant volume (8-10). The accuracy of MRI determinations of myocardial volumes (11) and myocardial hypertrophy may be particularly useful in the evaluation of volume overload conditions such as aortic insufficiency and pressure overload lesions. However, an important aspect of valvular heart disease centers around the visualization of the valve leaflets and the valve ring.

A recent review highlights the lack of published MRI data demonstrating valve leaflet morphology (2). MRI reports with a specific emphasis on cardiac valve leaflets have described 8 cases of Ebstein's anomaly (12,13), two aortic vegetations (14), and a quadricuspid aortic valve (15). Recent work with rapid acquisitions has demonstrated valve leaflets in a limited number of normal subjects (16,17) and three individuals with mitral valve disease (17).

The purpose of this study was to evaluate prospectively the ability of double inversion recovery fast spin-echo MRI to visualize the leaflets in suspected normal aortic valves. In addition, a limited number of other valves were imaged including seven cases of bicuspid or thickened aortic valves.

MATERIALS AND METHODS

In all, 120 subjects were imaged in a prospective study. Five patients were repeated 1 week to 6 months after the initial examination. Patients were all referred for cardiac MRI to evaluate myocardial mass or left ventricular volumes. These patients had conditions including hypertrophic cardiomyopathy, coronary artery disease, valvular heart disease, and right ventricular dysplasia. The five normal volunteers had no known heart disease and otherwise normal cardiac MRI studies. Clinical characteristics are listed in Table 1. Patients ranged in age from 9 to 75 years old (average 37) and included 86 males and 36 females. Heart rate ranged from 43 to 100 beats per minute.

¹Laboratory of Cardiac Energetics, National Heart, Lung, and Blood Institute, National Institutes of Health, Bethesda, Maryland 20892-1061.

²Applied Science Laboratory, General Electric Medical Systems, Waukesha, Wisconsin 53188.

³Integrated Cardiovascular Therapeutics, Woodbury, New York 11797. Contract grant sponsor: National Institutes of Health; Contract grant number: K08 HL03135.

Presented in part at the 70th Scientific Session of the American Heart Association, November 1997.

*Address reprint requests to: A.E.A., Laboratory of Cardiac Energetics, National Heart, Lung, and Blood Institute, National Institutes of Health, Bldg 10, Rm B1D416, MSC 1061, 10 Center Drive, Bethesda, MD 20892-1061.

Received May 12, 1998; Accepted May 28, 1999.

© 1999 Wiley-Liss, Inc.

Table 1
Patient Characteristics*

Parameter	Mean \pm SD	Range
Age (years)	37 \pm 14	9–75
Sex (male/female)	86/36	
Heart rate (bpm)	64 \pm 8	43–100
Breathhold time (sec)	15 \pm 3	9–22

*bpm = beats per minute.

A double inversion recovery preparation followed by a delayed fast spin-echo (FSE) readout produces black blood images as follows (18,19). First, a cardiac gated non-selective inversion pulse is applied, inverting the whole body. Next a slice-selective inversion pulse restores the magnetization state of the slice of interest but leaves the blood outside the slice inverted. During the inversion time, two factors lead to making the blood appear dark during the subsequent FSE readout: a) the magnetization of blood that started out of the slice is nulled and thus dark, and b) blood that started within the slice is replaced by dark blood from outside the slice.

Imaging was performed on a 1.5 T MRI scanner (General Electric, Milwaukee, WI). Gradients were operated at 77 T \cdot m⁻¹ \cdot sec⁻¹ slew rates and gradient amplitudes of 4 gauss \cdot cm⁻¹. Imaging parameters used in the first 34 subjects are summarized in Table 2. These values are representative of the entire population studied. Acquisitions were performed during breathholds that averaged 15 \pm 3 seconds and were triggered off every second heart beat. Triggering was near the peak of the QRS complex. With an average inversion time of 600 msec, the FSE readout typically occurred during mid-diastole for the heart rates encountered. Echo time was kept short to maximize signal, which was expected to be small for the thin leaflets. The echotrain length ranged from 20 to 32, resulting in a readout time of approximately 100–150 msec. Image resolution and breathhold time were individualized for each patient within their capabilities. The image resolution obtained was on average about 1.3 \times 1.3 mm in-plane with an average slice thickness of 4 mm. Receiver bandwidth was 62.5 kHz. A long-axis image through the ascending aortic root was prescribed from sagittal localizers. Next, between three and eight contiguous short-axis imaging planes were obtained to encompass the aortic valve.

Images were reviewed on the scanner console and on film. For qualitative reading, more than 80% of the valve leaflet from the central coaptation point to the aortic

Table 2
Imaging Parameter Summary

Parameter	Mean \pm SD	Range
Repetition time (msec)	1801 \pm 235	1411–2553
Echo time (msec)	23 \pm 9	15.3–42
Inversion time (msec)	600 \pm 47	502–716
Trigger delay (msec)	611 \pm 47	513–727
Field of view (cm)	33.5 \pm 3.6	24–48
Slice thickness (mm)	4.0 \pm 0.2	3–4

wall had to be visualized as a linear structure. Neighboring slices were used to trace leaflets not meeting these criteria within a single imaging plane. The signal-to-noise and contrast-to-noise ratios were measured in 15 randomly selected cases. Regions of interest were used to measure signal intensity of the valve leaflets, the aortic anulus, the blood in the aortic root, and air free of phase artifacts to represent noise. Contrast-to-noise ratio was calculated as the signal difference to noise ratio comparing blood in the aortic root with the valve leaflets and the walls of the aortic root.

Functional correlation to the diastolic black blood imaging was performed in a limited number of studies. A velocity-encoded segmented gradient-recalled echo sequence was used to encode for velocity through the imaging plane (20). These acquisitions used a repetition time of \approx 10 msec and an echo time of 4 msec and had a spatial resolution of about 1.4 \times 2.1 mm in-plane and a temporal resolution of about 80 msec. A systolic image was selected by determining the peak velocity through the aortic valve.

Statistics were calculated using Microsoft Excel for Windows 97. A paired two-tailed *t*-test was used to compare groups. The Bonferroni correction was used to account for multiple comparisons. Results are presented as mean \pm standard deviation.

RESULTS

In 102 of 120 studies (85%), all three leaflets were visualized. Seven subjects had distorted or thickened valves consistent with a bicuspid aortic valve. Echocardiography confirmed bicuspid aortic valves or abnormal leaflet morphology in five of these subjects and incompletely visualized the leaflets in the remaining two individuals. In the remaining studies, the aortic leaflets appeared thin and the three leaflets appeared radially symmetric around the center of the aortic root both in length and in terms of dividing the aortic root into roughly equal sized regions. This morphology is as expected for normal aortic valves.

The signal-to-noise ratio of the valves was 14 \pm 5, which is significantly higher than the signal-to-noise ratio of the residual blood signal around the aortic valve leaflets ($P < 0.001$) and significantly lower than for the walls of the aortic root ($P < 0.001$, Table 3). The contrast-to-noise ratio between blood and the valve

Table 3
Signal-to-Noise and Contrast-to-Noise Ratios for Aortic Valve Leaflets

Ratio	Mean \pm SD
Signal-to-noise	
Aortic valve leaflets	14 \pm 5*
Blood near aortic valve	7 \pm 4
Aortic root wall	43 \pm 12
Contrast-to-noise	
Leaflet vs. blood	7 \pm 5**
Aortic root wall vs. blood	36 \pm 12

* $P < 0.001$ vs. blood or aortic root wall.

** $P < 0.001$ vs. aortic root wall.

leaflets was much lower than for the walls of the aortic root ($P < 0.001$).

A black blood image of a normal aortic valve leaflets are shown in Fig. 1a (**E1336). Corresponding magnitude and velocity-encoded images are shown in Fig.

1b-d. Figure 2a shows the diastolic black blood images of a congenitally abnormal aortic valve in the same orientation as the corresponding systolic magnitude (Fig. 2b) and velocity images (Fig. 2c). Additional imaging planes for the example of a congenitally malformed

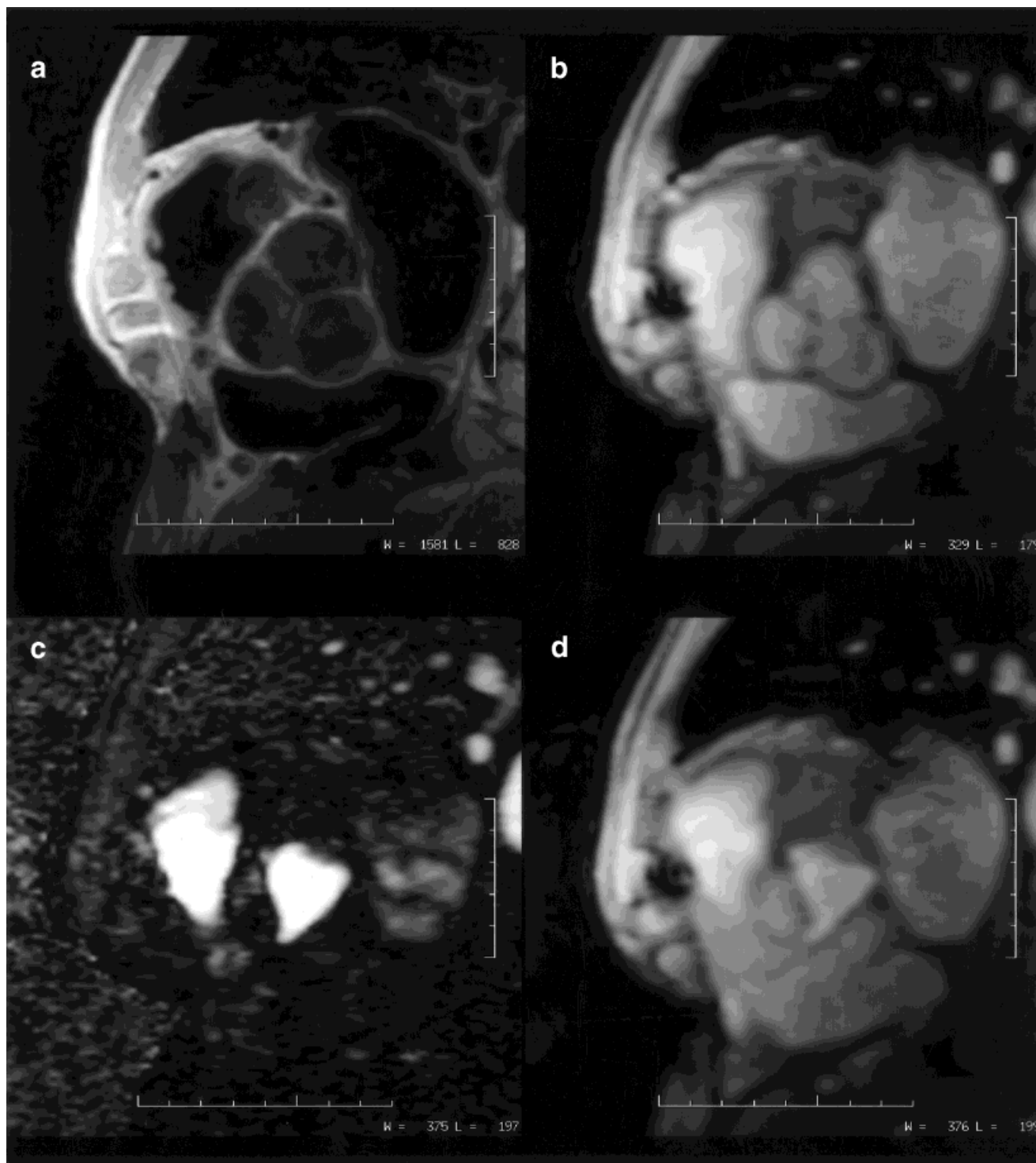


Figure 1. Normal aortic valve. **a.** Black blood image of a normal trileaflet aortic valve from a 79-year-old man with coronary artery disease, a dilated aortic root, and deformed chest after sternotomy. **b:** Magnitude gradient echo image in diastole. **c:** Velocity-encoded image of triangular aortic outflow in systole. (White represents high velocity, black represents low velocity, and random signal occurs where signal is low.) **d:** Magnitude gradient-echo image in systole.

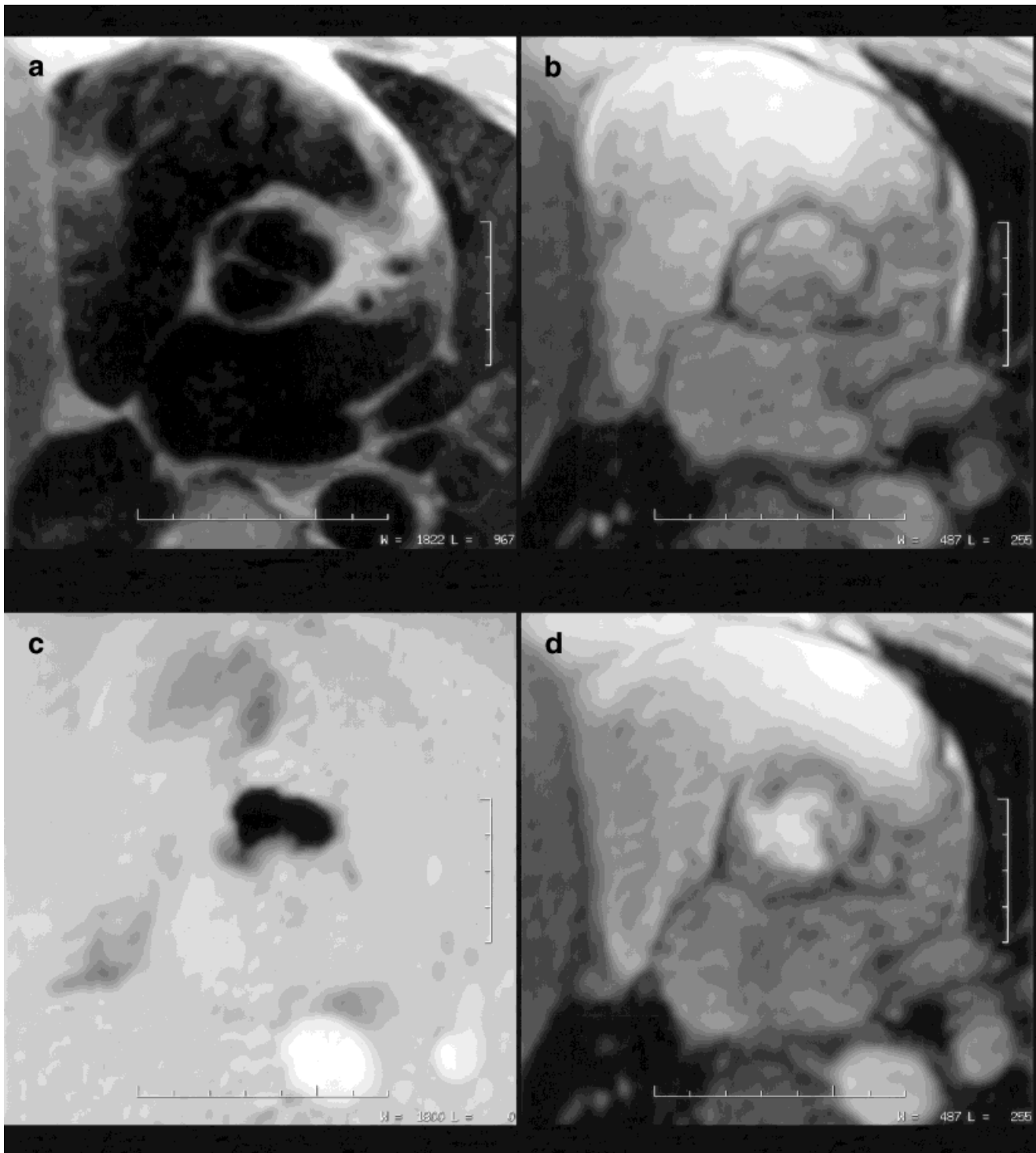


Figure 2. Congenitally malformed aortic valve. **a:** Diastolic black blood image demonstrating thin leaflets with markedly asymmetric coaptation point in a 48-year-old man with hypertrophic cardiomyopathy. **b:** Magnitude gradient-echo image in diastole. **c:** Velocity-encoded image during systole. The velocity pattern reveals a predominately oval appearance of the aortic orifice of a bicuspid valve with fusion of the right and left coronary leaflets. The abnormally short noncoronary and left coronary leaflets appear to open slightly, contributing to asymmetry of the flow pattern. In the velocity-encoded images, black represents high velocity through the imaging plane toward the head, white represents high velocity toward the feet, and gray represents zero velocity. Note that this image was masked by the magnitude image to suppress random speckle from areas with low signal intensity. **d:** Magnitude gradient-echo image in systole.

aortic valve are shown in Fig. 3. Figure 4 shows a bicuspid aortic valve due to fusion of the right and non-coronary leaflets.

DISCUSSION

This report summarizes our initial experience in visualizing the aortic leaflets in patients who mostly had normal aortic valves. In a prospective blinded study of 120 scans, all three leaflets were visualized in 85% of studies. The image quality as a group was sufficient to assess qualitatively both the eccentricity of the central coaptation point and the relative leaflet lengths. In this experience, seven cases of bicuspid or abnormal aortic valve were easily detected in a blinded reading and verified by echocardiography in five. Thus, MRI appears to be a useful and less invasive alternative than transthoracic echocardiography for visualizing valve leaflet morphology when the transthoracic echo window is inadequate.

Preliminary experience suggests that the other valves can be imaged as well. An example of a sagittal image through the pulmonic valve and a short-axis view through the pulmonic valve is shown in Fig. 5. In addition to visualizing the leaflets, the double inversion recovery (IR) FSE provides high-resolution images of the valve annulus. This information could be used for sizing prosthetic valves. It has been argued that an *in vivo* measurement of the annular size can be on the order of 40% larger than that estimated in an unpressurized heart (21).

The use of a black blood imaging sequence such as double IR FSE displays the valves relatively bright compared with dark blood. This is a distinct advantage compared with bright blood imaging sequences. For example, valve leaflets can be seen in multiphase cine GRE images as relatively low signal intensity linear structures in contrast to the bright blood. However, normal flow-related signal intensity changes in the blood (22) and abnormal flow-related signal voids also appear as low signal intensity in the area of the valve. Furthermore, saturation of static blood in the area of the valve can reduce the conspicuity of the valves.

Cine GRE has the advantage of depicting leaflet motion. GRE imaging can depict calcification as a signal void, an important marker of significant valvular heart disease (23). Thus the double IR FSE sequence will need to be tested on patients with calcific valvular heart disease. GRE experiments are also necessary for velocity-encoded imaging sequences. It may be that double IR FSE and cine GRE will be used in a complementary way to evaluate abnormal valves more completely.

Multiphase black blood imaging is theoretically possible although some technical considerations would need to be resolved for other phases of the cardiac cycle. Obtaining a bright signal from the valve requires the myocardium of interest to be in the imaging slice during the reinversion and the FSE readout. A bright valve signal is also dependent on the relatively thin leaflet being in the same location on several heart beats. These conditions are satisfied with diastolic imaging at normal resting human heart rates. This requirement at other phases of the cardiac cycle would require additional

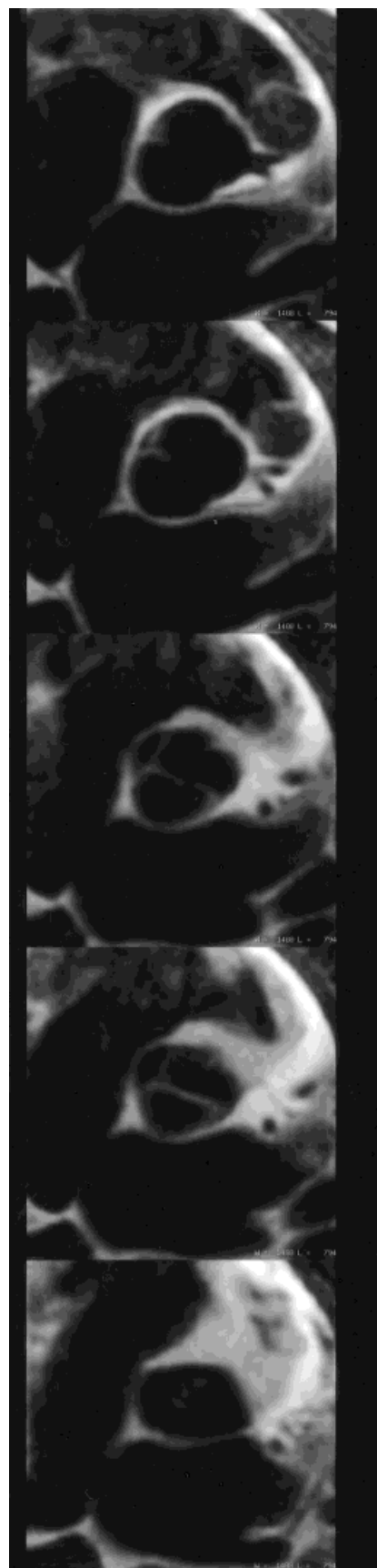


Figure 3. Additional imaging levels near the aortic root of the example shown in Fig. 2 demonstrating the valve orientation relative to the proximal coronary arteries and asymmetry of the leaflets in multiple imaging planes.

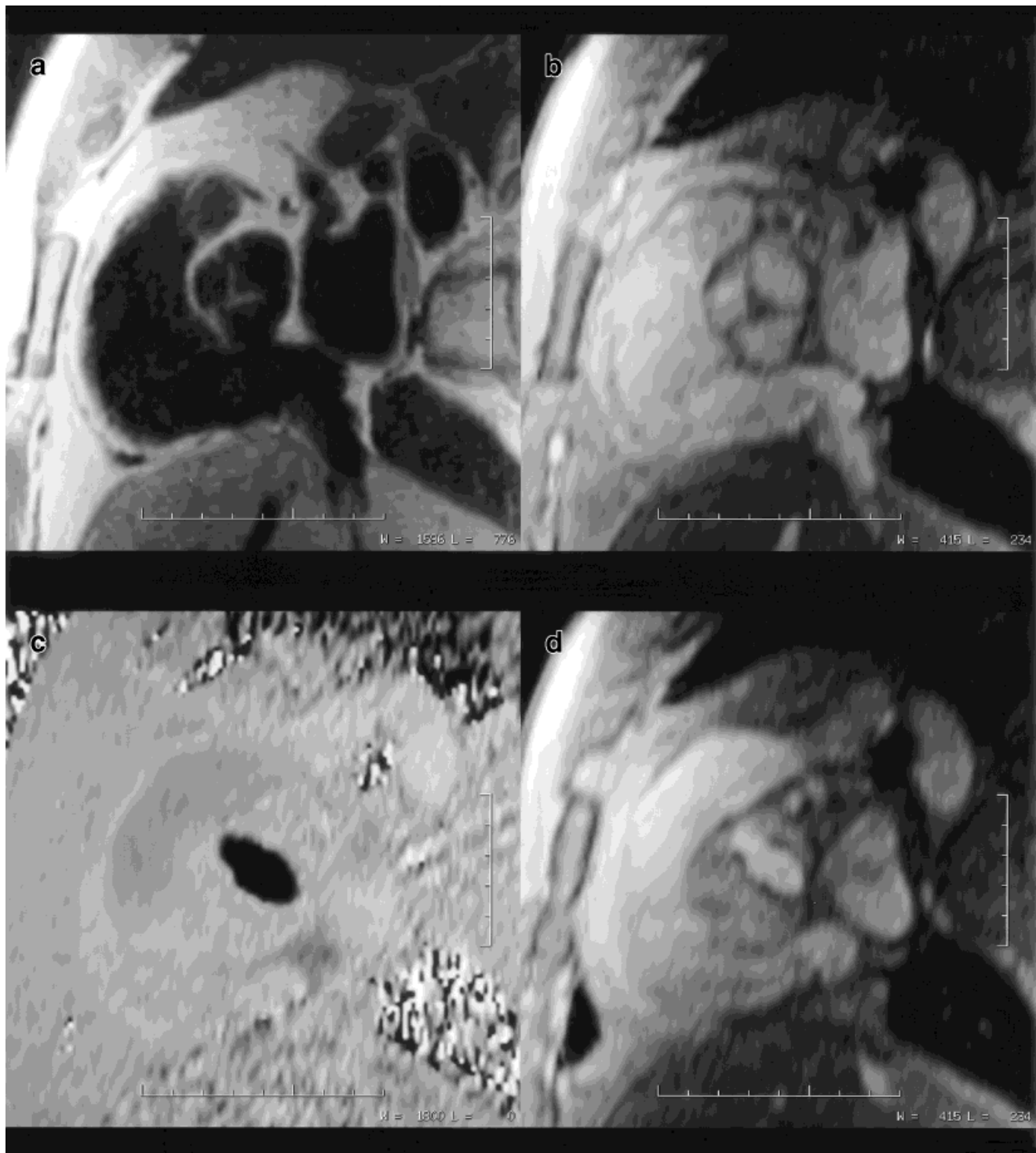


Figure 4. Bicuspid aortic valve due to leaflet fusion. **a:** Black blood image of a bicuspid aortic valve in an otherwise healthy 44-year-old man. The aortic leaflets appear thickened and markedly asymmetric. **b:** Magnitude gradient-echo image in diastole. **c:** Velocity-encoded image during systole. The velocity pattern reveals a typical oval appearance of the aortic orifice of a bicuspid valve with fusion of the right and non-coronary leaflets. **d:** Magnitude gradient-echo image in systole.

technical development. Finally, the FSE readout is approximately 100–150 msec for the selected echo train length and image resolution. Thus motion during this readout time would be expected to degrade image quality. Diastolic imaging of the aortic valve is practical

since these conditions can be met with an electrocardiographically triggered acquisition.

In summary, this work indicates the feasibility of directly imaging the aortic leaflets in a high fraction of patients. FSE cannot be expected to image all aspects of

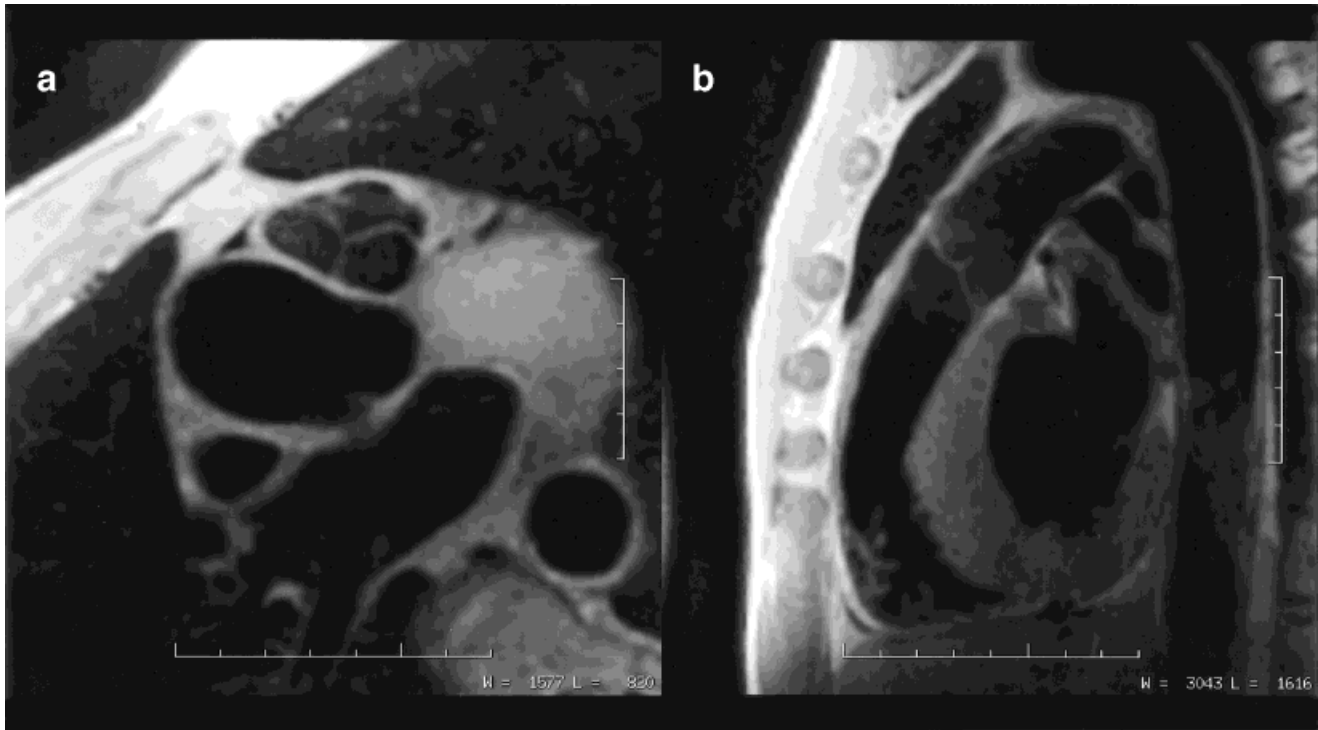


Figure 5. Black blood images of the pulmonic valve. **a:** Short-axis image of the pulmonic valve in a 38-year-old man with left ventricular hypertrophy due to hypertension. **b:** Long-axis image of pulmonic valve.

valvular heart disease, but the direct visualization of the leaflets at high resolution can complement methodologies that are good at imaging the physiological consequences of valvular abnormalities but have limited ability to visualize the valve leaflets themselves.

REFERENCES

- Globits S, Higgins CB. Assessment of valvular heart disease by magnetic resonance imaging. *Am Heart J* 1995;129:369–381.
- Wytenbach R, Bremerich J, Saeed M, Higgins CB. Integrated MR imaging approach to valvular heart disease. *Cardiol Clin* 1998;16:277–294.
- Kilner PJ, Firmin DN, Rees RS, et al. Valve and great vessel stenosis: assessment with MR jet velocity mapping. *Radiology* 1991;178:229–235.
- Yoshida K, Yoshikawa J, Hozumi T, et al. Assessment of aortic regurgitation by the acceleration flow signal void proximal to the leaking orifice in cinemagnetic resonance imaging. *Circulation* 1991;83:1951–1955.
- Heidenreich PA, Steffens J, Fujita N, et al. Evaluation of mitral stenosis with velocity-encoded cine-magnetic resonance imaging. *Am J Cardiol* 1995;75:365–369.
- Globits S, Frank H, Mayr H, Neuhold A, Glogar D. Quantitative assessment of aortic regurgitation by magnetic resonance imaging. *Eur Heart J* 1992;13:78–83.
- Hundley WG, Li HF, Willard JE, et al. Magnetic resonance imaging assessment of the severity of mitral regurgitation. Comparison with invasive techniques. *Circulation* 1995;92:1151–1158.
- Sondergaard L, Hildebrandt P, Lindvig K, et al. Valve area and cardiac output in aortic stenosis: quantification by magnetic resonance velocity mapping. *Am Heart J* 1993;126:1156–1164.
- Sechtem U, Pflugfelder PW, Cassidy MM, et al. Mitral or aortic regurgitation: quantification of regurgitant volumes with cine MR imaging. *Radiology* 1988;167:425–430.
- Sondergaard L, Lindvig K, Hildebrandt P, et al. Quantification of aortic regurgitation by magnetic resonance velocity mapping. *Am Heart J* 1993;125:1081–1090.
- Sakuma H, Globits S, Bourne MW, et al. Improved reproducibility in measuring LV volumes and mass using multicore breath-hold cine MR imaging. *J Magn Reson Imaging* 1996;6:124–127.
- Link KM, Herrera MA, D'Souza VJ, Formanek AG. MR imaging of Ebstein anomaly: results in four cases. *AJR Am J Roentgenol* 1988;150:363–367.
- Choi YH, Park JH, Choe YH, Yoo SJ. MR imaging of Ebstein's anomaly of the tricuspid valve. *AJR Am J Roentgenol* 1994;163:539–543.
- Caduff JH, Hernandez RJ, Ludomirsky A. MR visualization of aortic valve vegetations. *J Comput Assist Tomogr* 1996;20:613–615.
- Kajinami K, Takekoshi N, Mabuchi H. Images in cardiology. Non-invasive detection of quadricuspid aortic valve. *Heart* 1997;78:87.
- Frahm J, Merboldt KD, Bruhn H, et al. 0.3-second FLASH MRI of the human heart. *Magn Reson Med* 1990;13:150–157.
- Davis CP, McKinnon GC, Debatin JF, Duewelle S, von Schulthess GK. Single-shot versus interleaved echo-planar MR imaging: application to visualization of cardiac valve leaflets. *J Magn Reson Imaging* 1995;5:107–112.
- Edelman RR, Chien D, Kim D. Fast selective black blood MR imaging. *Radiology* 1991;181:655–660.
- Simonetti OP, Finn JP, White RD, Laub G, Henry DA. "Black blood" T2-weighted inversion-recovery MR imaging of the heart. *Radiology* 1996;199:49–57.
- Feinstein JA, Epstein FH, Arai AE, et al. Using cardiac phase to order reconstruction (CAPTOR): a method to improve diastolic images. *J Magn Reson Imaging* 1997;7:794–798.
- Vesely I, Menkis AH, Rutt B, Campbell G. Aortic valve/root interactions in porcine hearts: implications for bioprosthetic valve sizing. *J Card Surg* 1991;6:482–489.
- Mirowitz SA, Lee JK, Gutierrez FR, Brown JJ, Eilenberg SS. Normal signal-void patterns in cardiac cine MR images. *Radiology* 1990;176:49–55.
- Pucillo AL, Schechter AG, Kay RH, Moggio R, Herman MV. Identification of calcified intracardiac lesions using gradient echo MR imaging. *J Comput Assist Tomogr* 1990;14:743–747.